geologicaacta

Citation: Ruh, J.B., 2025. Grain-size reduction reduces the impact of viscous shear heating in lithospheric mantle shear zones. Geologica Acta, 23.26, 1-pgs. DOI: 10.1344/GeologicaActa2025.23.26
Online ISSN: 1696-5728

Grain-size reduction reduces the impact of viscous shear heating in lithospheric mantle shear zones

J.B. Ruh

Instituto de Ciencia del Mar, Consejo Superior de Investigaciones Científicas (CSIC)
Barcelona, Spain. E-mail: jruh@icm.csic.es

ABSTRACT

Active plate tectonics require weak boundaries that accommodate large strain over long time periods. Many studies argue that shear heating converted from dissipated mechanical energy may be responsible for the necessary weakening in the mantle lithosphere to initiate and sustain weak plate boundaries. Here, I present simple numerical simulations of pure olivine systems with a composite diffusion-dislocation creep rheology coupled to a self-consistent grain-size evolution model to investigate the effect of grain-size reduction on shear heating. Results demonstrate that the weakening related to grain-size reduction and the activation of grain-size-sensitive diffusion creep undermines the importance of shear heating in mantle shear zones. Depending on shear zone width, shear velocity and apparent stresses, estimations on ideal shear zone widths and viscosities are presented.

KEYWORDS **Shear heating. Grain-size evolution. Rheology. Shear zones. Numerical modelling.**

INTRODUCTION

Localization of deformation in the Earth's lithosphere is an essential ingredient for active plate tectonics, where strong, relatively undeformed plates are bounded to each other along mechanically relatively weak boundaries (Bercovici *et al.*, 2000; Gurnis *et al.*, 2000). In this regard, long-term strain localization at plate boundaries requires a certain amount of mechanical weakening of the lithosphere (Frederiksen and Braun, 2001; Holyoke and Tullis, 2006). Weakening and consequent strain localization in the lithosphere have been proposed to be the result of a variety of processes acting individually or concurrent, such as an increase in fluid concentration (Alevizos *et al.*, 2014; Wibberley and Shimamoto, 2005), metamorphic reactions leading to growth of weaker phases (Ceccato *et al.*, 2018; Oliot *et al.*, 2010), fabric development during shearing (Montesi, 2013; Rast and Ruh, 2021), shear heating (Duretz *et al.*, 2015; Kaus and Podladchikov, 2006; Thielmann and Kaus, 2012) and grain-size reduction and the subsequent activation of diffusion creep (Platt and Behr, 2011; Ruh *et al.*, , 2022, 2024; Warren and Hirth, 2006).

Many studies pointed out the effect of shear heating on overall lithospheric strength (Hartz and Podladchikov, 2008), temperature-related metamorphism (Burg and Gerya, 2005), and its role during the initiation of subduction (Thielmann and Kaus, 2012). Although there is a consensus that different weakening processes may act simultaneously, their individual effects on each other have often been neglected. Potential negative feedback effects are particularly important for shear heating, as it is derived from the deformational dissipation energy, which depends on the apparent stress state in a shear zone (Brun and Cobbold, 1980; Yuen *et al.*, 1978). Vice versa, a temperature increase due to shear heating affects the viscosity and grain-growth rate in shear zones (Hirth and Kohlstedt, 2003; Speciale *et al.*, 2020). Recent studies have furthermore shown that shear heating combined with grain-size reduction may explain the occurrence of thermal

runaway and intermediate depth seismicity (Spang *et al.*, 2024, 2025; Thielmann *et al.*, 2015).

Here, I present numerical simulations that couple a composite dislocation and diffusion creep flow law with a self-consistent Grain-Size Evolution (GSE) model for olivine to investigate the effects of grain-size reduction on shear heating and the localization of ductile shear zones in the lithospheric mantle. I thereby take advantage of a recently published growth law for olivine (Speciale *et al.*, 2020) and new estimations on the partitioning factor that determines how much of the work done in dislocation creep goes into grain-size reduction (Holtzman *et al.*, 2018; Ruh *et al.*, 2022).

METHODS

Composite rheology, grain-size evolution and heat budget

The coupled thermo-mechanical grain-size evolution model is calculated for constant strain rates or stresses expected to occur in olivine-bearing lithospheric shear zones. The composite viscous relationship of stress and strain rate depends on grain-size-independent dislocation and grain-size-dependent diffusion creep for wet olivine (Hirth and Kohlstedt, 2003):

$$\dot{\varepsilon}_{tot} = \dot{\varepsilon}_{dis} + \dot{\varepsilon}_{dif} \quad (1)$$

where

$$\dot{\varepsilon}_i = A_i \cdot f_{H_2O}^{r_i} \cdot \sigma^{n_i} \cdot d^{-m_i} \cdot \exp\left(-\frac{E_i + P \cdot V_i}{RT}\right) \quad (2)$$

with $\dot{\varepsilon}_1 = \dot{\varepsilon}_{dis}$ and $\dot{\varepsilon}_2 = \dot{\varepsilon}_{dif}$ A is a pre-exponent, f_{H_2O} is fugacity, r is the fugacity exponent, σ is stress, n is the stress exponent, d is grain size, m is the grain-size exponent, E is activation energy, P is pressure, V is activation volume, R is the gas constant and T is temperature (see Table 1).

Grain-size evolution is implemented based on the paleowattmeter (Austin and Evans, 2007, 2009), where the total grain-size change rate depends on independent terms for grain-size reduction rate, $\dot{d}_{red}$, and grain-growth rate, $\dot{d}_{gr}$:

$$d = d_{old} + (\dot{d}_{gr} - \dot{d}_{red}) \cdot dt \quad (3)$$

dold and *d* are old and new grain sizes, and *dt* the time step. Grain-size reduction, $\dot{d}_{red}$, depends on the fraction λ of energy dissipated by dislocation creep ($\sigma \dot{\varepsilon}_{disi}$) going into grain-size reduction, a grain-shape parameter, c, and grain-boundary energy, γ (see Table 1):

$$\dot{d}_{red} = \frac{\sigma \dot{\varepsilon}_{disi} \lambda d_{old}^2}{c\gamma} \quad (4)$$

Recent studies demonstrated that the fraction of dissipation energy produced by dislocation creep that goes into grain-size reduction is significantly smaller than previously thought. A fraction of λ= 0.1 was often interpreted based on studies investigating metals that showed that ~90% of the dissipated energy goes converts into heat (Austin and Evans, 2009; Hodowany *et al.*, 2000). However, recent work based on experimental data and thermodynamics suggested lower values of λ for natural rocks (Holtzman *et al.*, 2018; Tokle and Hirth, 2021). Here, I apply a value of λ= 0.01, which is consistent with recent findings for natural olivine (Ruh *et al.*, 2022).

Olivine grain growth, $\dot{d}_{gr}$, depends on a temperature-dependent growth term, $K_g \cdot f_{H_2O} \cdot \exp\left(\frac{-E_g + P \cdot V_g}{RT}\right)$, and a growth exponent, p (see Table 1):

$$\dot{d}_{gr} = K_g \cdot f_{H_2O} \cdot \exp\left(\frac{-E_g + P \cdot V_g}{RT}\right) \cdot p^{-1} \cdot d_{old}^{1-p} \quad (5)$$

Speciale *et al.* (2020) suggest that growth of natural olivine is significantly slower than the often-applied fast growth law by Karato (1989). In fact, applying Karato's (1989) graingrowth law of olivine hampers grain-size reduction drastically and does not allow for the activation of grain-size-dependent diffusion creep in the upper mantle (Ruh *et al.*, accepted), which is inconsistent with natural observations of diffusional creep processes in fine-grained olivine-bearing lithospheric mantle shear zones (*e.g.* Hodowany *et al.*, 2019). Here, I implement the recent growth law by Speciale *et al.* (2020) that allows for grain-size reduction necessary to activate diffusion creep in localized shear zones.

The temperature evolution of lithospheric shear zones is described by thermal diffusion, viscous shear heating and heat produced during grain growth (Thielmann *et al.*, 2015):

$$\rho C_p \frac{\partial T}{\partial t} = \kappa \frac{\partial^2 T}{\partial L^2} + (1-\lambda) \cdot \sigma \dot{\varepsilon}_{dis} + \sigma \dot{\varepsilon}_{dif} + \frac{\gamma \cdot K_g \cdot f_{H_2O} \cdot \exp\left(\frac{-E_g + P \cdot V_g}{RT}\right)}{p \cdot d^{p-1}} \quad (6)$$

where ρ is density, *Cp* is heat capacity, κ is heat diffusivity, and *L* is the width of the shear zone (see Table 1). The heat equation derivative is replaced by a simple second-order finite difference approximation across a width *L*:

$$\kappa \frac{\partial^2 T}{\partial L^2} \approx \frac{T_{bg} - 2T_{sz} + T_{bg}}{\Delta L^2} \quad (7)$$

which allows the temperature evolution in the shear zone to be defined as

$$T_{sz}^{new} = T_{sz} + \left(\frac{\kappa}{\rho C_p} \frac{2(T_{bg} - T_{sz})}{L^2} + \frac{(1-\lambda) \cdot \sigma \dot{\varepsilon}_{dis}}{\rho C_p} + \frac{\sigma \dot{\varepsilon}_{dif}}{\rho C_p} + \frac{\gamma \cdot K_g \cdot f_{H_2O} \cdot \exp\left(\frac{-E_g + P \cdot V_g}{RT}\right)}{\rho C_p \cdot p \cdot d^{p-1}}\right) \cdot dt \quad (8)$$

Tsz is the temperature in the shear zone and *Tbg* is the background temperature outside the shear zone.

TABLE 1. Rheological, thermal and grain-size evolution parameters (Austin and Evans, 2007; Burg and Gerya, 2005; Clauser and Huenges, 1995; Duyster and Stöckhert, 2001; Hirth adn Kohlstedt, 2003; Speciale *et al.*, 2020; Turcotte and Schubert, 2002)

Dislocation creep		
A_{disl} (Pa^{-n-p})	$9 \cdot 10^{-20}$	Hirth and Kohlstedt (2003)
n_{disl} (-)	3.5	
m_{disl} (-)	0	
r_{disl} (-)	1.2	
E_{disl} (kJ/mol)	480	
V_{disl} (m^3/mol)	$11 \cdot 10^{-6}$	

Diffusion creep		
A_{diff} (Pa^{-n-p})	$1 \cdot 10^{-27}$	Hirth and Kohlstedt (2003)
n_{diff} (-)	1	
m_{diff} (-)	3	
r_{diff} (-)	1	
E_{diff} (kJ/mol)	335	
V_{diff} (m^3/mol)	$4 \cdot 10^{-6}$	

Thermal diffusion		
ρ (kg/m^3)	3300	Turcotte and Schubert (2002)
C_P (J/kg/K)	1000	Burg and Gerya (2005)
k (W/m/K)	0.73 + (1293/T +77)*	Clauser and Huenges (1995)

* T is temperature in K

Grain size reduction		
c (-)	3.1415	Austin and Evans (2007)
γ (J/m^2)	1.4	Duyster and Stöckert (2001)
Λ (-)	0.01	Ruh *et al.* (2022)

Grain growth		
K_g (m^p/s)*	3	Speciale *et al.* (2020)
p (-)	3.2	
E_g (kJ/mol)	620	
V_g (m^3/mol)	$5 \cdot 10^{-6}$	

Modelling strategy

A suite of zero-dimensional simulations are run for either constant strain rate or constant stress. Shear zone width is defined by the relationship between shear strain rate and the bulk shear velocity (boundary conditions):

$$L = \frac{V_s}{\dot{\varepsilon}} \quad (9)$$

All simulations are conducted for constant shear velocities *vs* of 3.16mm/yr or 3.16cm/yr, representing first-order estimations of natural plate boundary velocities. This implies that simulations at constant stress may result in variable strain rates according to equation (2), affecting shear zone width (equation 9) and ultimately thermal diffusion (equation 6). Simulations at constant strain rates maintain their width over time.

In a first series of simulations, the temporal evolution of pure olivine shear zones is conducted at mantle lithospheric conditions with an initial temperature of 800°C, a pressure of 1.65GPa and a hydrogen concentration of C_{OH}= 50H/10^{6}Si. Simulations are run at various constant stresses (σ= 30, 40, 50MPa). To assess the effect of grain-size reduction on shear heating and thermo-mechanical weakening, all simulations are run both with a dynamic grain-size evolution and at constant grain sizes. Initial grain size is 5mm, comparable to observations from low strain mantle xenoliths (Dygert *et al.*, 2019). Additionally, a suit of simulations at variable constant stresses and boundary velocities for temperatures of T= 800 and 1100°C and hydrogen concentrations of C_{OH}= 50 and 600H/10^{6}Si are conducted that allow estimations on natural shear zone width and viscosities.

In a second series of simulations, the temporal evolution of shear zones is calculated at constant strain rates ($\dot{\varepsilon}$= 10^{-14}, 10^{-13}, 10^{-12}s^{-1}), with an initial temperature of 800°C, a pressure of 1.65GPa and a hydrogen concentration of C_{OH} = 50H/10^{6}Si. Additionally, simulations for variable constant strain rates, boundary velocities and hydrogen concentrations are run for temperatures and pressures between 600 to 1200°C and 1 to 3GPa, respectively, representing a vertical profile across a mantle lithosphere. Results from such simulations allow constructing vertical strength profiles and retrieving acting boundary forces (integrated strength profiles). The temporal evolution of shear zone temperature is calculated for both cases of constant grain size and dynamic grain-size evolution depending on hydrogen concentration, shear velocity, and strain rate.

RESULTS

Shear zone evolution at constant stress

Figure 1 illustrates the temporal evolution of grain size, percentage of diffusion creep of the total strain rate, strain rate and temperature of shear zones at constant stress for constant grain sizes (Fig. 1A-C) and with a self-consistent grain-size evolution model (Fig. 1D-G). In case of constant grain sizes of 5mm, deformation is dominated by dislocation creep (Fig. 1A) and strain rates do not indicate intense strain localization (Fig. 1B). Temperature increase related to shear heating varies from some degrees for a stress of 30MPa to ~60°C at 50MPa, where steady state is reached, *i.e.* temperature production by shear heating and loss related to diffusion is balanced (Fig. 1C). Temporal evolution of simulations including GSE show a rapid decrease of grain size to ~20–50μm at 30–50MPa (Fig. 1D), leading to diffusion creep dominating long-term deformation (Fig. 1E). Temperature anomalies produced by shear heating are significantly lower than for simulations with a constant grain size, showing an initial peak and long-term values <10°C at 30–50MPa, respectively (Fig. 1G). In general, steady-state strain rate and temperature conditions establish after ~3Myr at 50MPa and >10Myr at 30MPa, where temperature diffusion and shear heat production are balanced (Fig. 1F, G).

Shear zone width calculated from the strain rate (equation 9) after acquiring steady state is illustrated depending on constant applied stress and shear velocity *vs* for simulations at T= 800 and 1100°C and C_{OH}= 50 and 600H/10^{6}Si (Fig. 2A-D). Generally, slower velocities and larger stresses lead to narrower shear zone widths. At a temperature of 800°C and a hydrogen concentration of 50H/10^{6}Si, ideal shear zone width for *vs*= 3cm/yr and σ= 20MPa is ~2km, while for *vs*= 1mm/yr and σ= 50MPa it is ~7m (Fig. 2A). Simulations at 1100°C and 50H/10^{6}Si result in shear zone widths between 1 to 20km, for stresses between 2 and 5MPa (Fig. 2C). An increase in hydrogen concentration from 50 to 600H/10^{6}Si results in a decrease in shear zone width of roughly one order of magnitude (Fig. 2B, D). The resulting shear zone viscosity is mainly dependent on the acting stress, while shear velocity has only a minor effect (Fig. 2E-H).

Shear zone evolution at constant strain rate

Figure 3 shows the temporal evolution of grain size, percentage of diffusion creep of the total strain rate, stress and temperature of shear zones at constant strain rate for constant grain sizes (Fig. 3A-C) and with a self-consistent grain-size evolution model (Fig. 3D-G). In case of constant grain sizes of 5mm, deformation is dominated by dislocation creep (Fig. 3A). Stresses do not significantly decrease in case of strain rates of 10^{-12} and 10^{-14}s^{-1}, showing little strain localization, whereas a drop of >50MPa occurs for strain rates of 10^{-13}s^{-1} (Fig. 3B). Temperature increase related to shear heating is directly relatable to the observed stress drops, reaching almost 100°C for strain rates of 10^{-13}s^{-1} (Fig. 3C). For simulations with GSE, grain sizes reduce rapidly to ~20–90μm for strain rates of 10^{-12} to 10^{-14}s^{-1} (Fig. 3D), resulting in diffusion creep being the dominant deformation mechanism (Fig. 3E). Stresses reduce within the first 1Myr to 5–10MPa (Fig. 3F). Shear heating is significantly reduced compared to simulations without GSE, resulting in steady-state temperature anomalies of ~2–13°C for strain rates between 10^{-12} and 10^{-14}s^{-1}, respectively (Fig. 3G).

Figure 4 illustrates the temporal evolution of the temperature anomaly induced by shear heating at constant grain size (Fig. 4A-D) and with GSE (Fig. 4E-H), together with the resulting strength profiles after 2Myr (Fig. 4I-L), for a typical vertical pressure-temperature profile across a continental lithosphere. Maximum shear heating occurs at

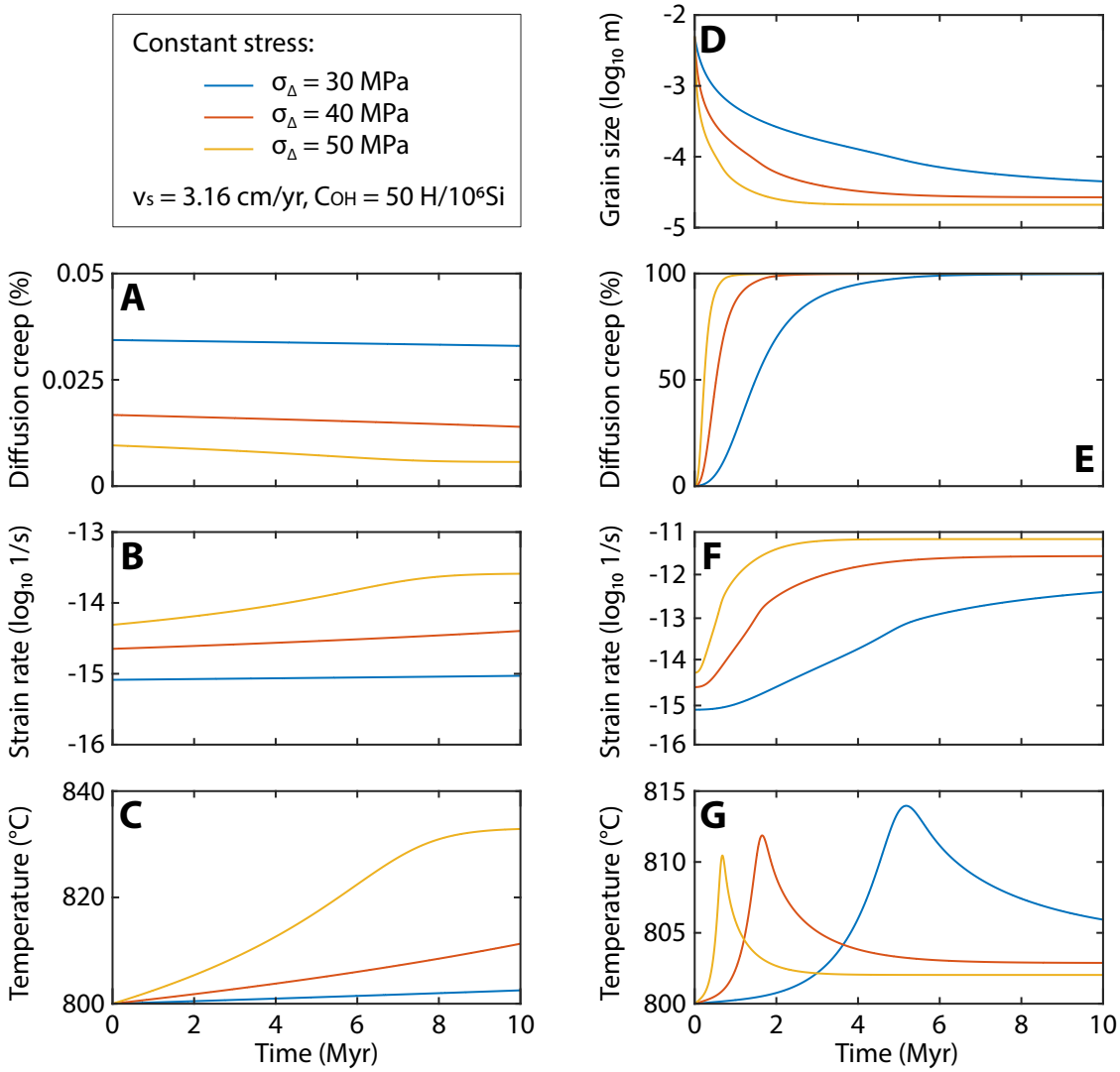

FIGURE 1. Temporal evolution of simulations at constant stress at PT conditions of 800°C and 1.65GPa, a shear velocity of 3.16cm/yr and hydrogen concentration of 50H/10^{6}Si. Left column: Constant grain size of 5mm. Right column: Self-consistent grain-size evolution. A, E) Percentage of diffusion creep adding to the total strain rate. B, F) Strain rate. C, G) Temperature. D) Grain size. Colors indicate applied stress.

shallow depths (T= 600°C) for all simulations. Compared to the simulation with $\dot{\varepsilon}$= 10^{-12}s^{-1}, vs= 3.16cm/yr and C_{OH}= 600H/10^{6}Si (Fig. 4A), an increase in hydrogen concentration and a decrease of shear velocity both result in reduced shear heating (Fig. 4B, C). Slower strain rates at equal shear velocity, *i.e.* wider shear zones, result in slower but more intense shear heating (Fig. 4D). For all cases, the activation of grain-size reduction leads to very effective weakening and a reduction of shear heating (Fig. 4E-H). Strength profiles indicate the lithospheric weakening induced by shear heating alone (red lines) and for a combined effect of (now reduced) shear heating and grain-size reduction (Fig. 4I-L). Even though shear heating can reduce stresses at shallow levels by several hundreds of MPa, grain-size reduction remains the main driver in weakening.

DISCUSSION

Effect of grain-size reduction on shear heating and shear zone strength

A comparison of simulations with constant grain sizes (5mm) versus ones with a self-consistent grain-size evolution clearly demonstrate the effect of grain-size reduction on shear heating and overall strength of an olivine-dominated mantle lithosphere. Independent on whether a constant stress or strain rate is assumed, work-related grain-size reduction rapidly activates diffusion creep and increases strain rates or reduces stresses, respectively (Fig. 1; 3). In both cases, shear heating is undermined by this effect: i) At constant stresses, increasing strain rates result in narrower shear zones and therefore faster heat

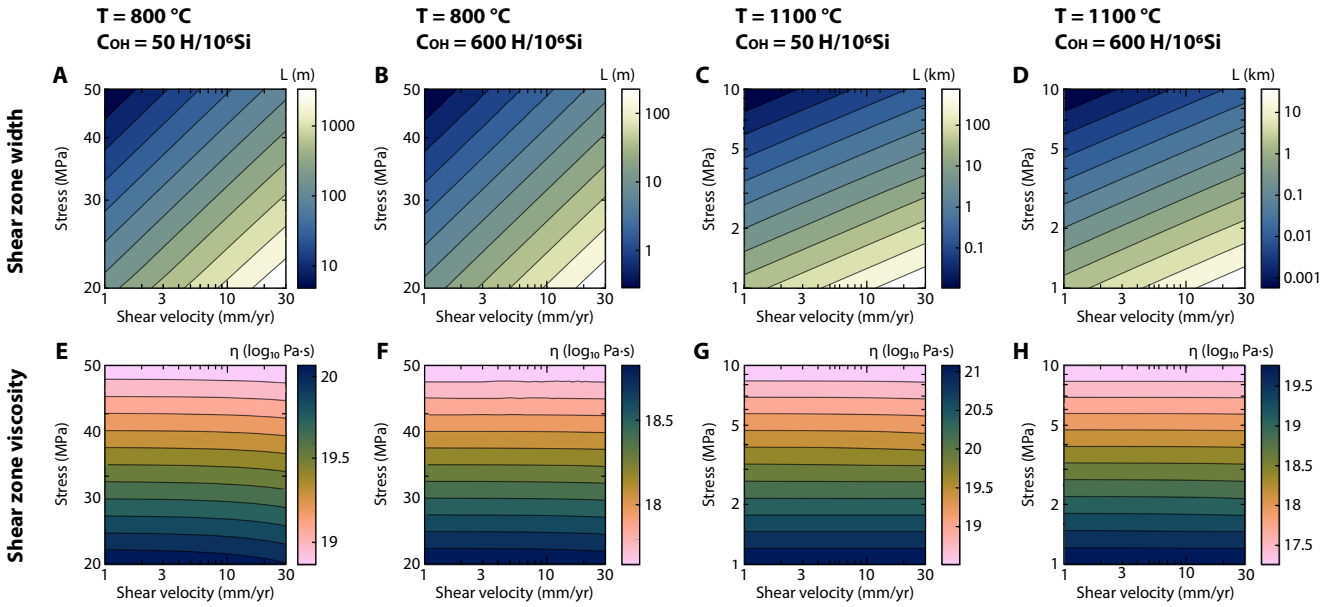

FIGURE 2. Ideal shear zone A-D) width and E-H) viscosity depending on applied stress and shear velocity after reaching steady-state conditions. PT conditions exhibit 800°C and 1.65GPa, with a hydrogen concentration of A,E) 50H/10⁶Si and B,F) 600H/10⁶Si, and 1100°C and 2.62GPa, with a hydrogen concentration of C,G) 50H/10⁶Si and D-H) 600H/10⁶Si. Shear zone widths are given in meters for (A and B) and in kilometer in (C and D).

loss by diffusion. ii) At constant strain rates (*i.e.* constant shear zone width), reduced stresses result in lesser shear heat production. However, independent of the induced shear heating within a shear zone, the consequent thermo-mechanical weakening remains a fraction of the weakening resulting from grain-size reduction and the activation of grain-size-sensitive diffusion creep (Fig. 4I-L).

Several studies pointed out the importance of shear heating for weakening and strain localization in the lithosphere (Burg and Gerya, 2005; Duretz *et al.*, 2015; Hartz and Podladchikov, 2008; Kaus and Podladchikov, 2006; Kiss *et al.*, 2020; Mako and Caddick, 2018; Schmalholz and Duretz, 2015; Thielmann and Kaus, 2012), while they are not negating that other processes such as grain-size reduction may also play an important role (Behn *et al.*, 2009; Bercovici and Ricard, 2012; Braun *et al.*, 1999; Dannberg *et al.*, 2017; De Bresser *et al.*, 2001; Fuchs and Becker, 2021; Jain *et al.*, 2018; Platt, 2015; Schierjott *et al.*, 2020). Kiss *et al.* (2020) for example demonstrated that temperature anomalies related to shear heating may reach >200°C, significantly weakening the uppermost mantle lithosphere. In this regard, the present study shows that shear heating within shear zones is hampered by strength loss due to grain-size reduction (Fig. 4A-H). However, Thielmann *et al.* (2015) showed that shear heating up to melting point temperatures can develop locally in case of seismic velocities. But there, thermal anomalies occur as transient processes and are dependent on either higher stress or faster strain rates than discussed here. Here, I demonstrate that thermal anomalies, and therefore temperature-related weakening, are largely restricted to the upper part of the mantle lithosphere.

Temporal evolution of boundary forces, *i.e.* vertically integrated mantle lithospheric strength, shows that without a sophisticated grain-size evolution, values of up to 30TN/m are necessary to maintain large-scale shear zones at given strain rates (Fig. 5). On the other hand, grain-size reduction and consequent weakening reduces boundary forces below 2TN/m within less than half a million years for variable strain rates and shear velocities (Fig. 5), comparable to typical values interpreted to act along plate boundaries and thus allowing for the localization of strain along those (Bird *et al.*, 2008; Gurnis *et al.*, 2004).

Natural constrains of shear heating

Simulations of pure wet olivine rheologies presented in this study suggest that shear heating in the upper mantle is of minor importance and thermal anomalies above 10–20°C are not expected (Fig. 4E-H). However, this does not imply that shear heating is absent throughout the lithosphere. Studies on natural shear zones have shown that maximum temperatures may be significantly increased relative to the surrounding, undeformed host rock. For example, Camacho *et al.* (2001) reported temperature anomalies of ~200°C in eclogite facies shear zones from central Australia. This may be explained by granulite and eclogite rheologies that are significantly stronger than wet olivine (Jin *et al.*, 2001), hence resulting in larger stresses and increased shear heating. Also Kienast and Leloup (1993; see also Leloup *et*

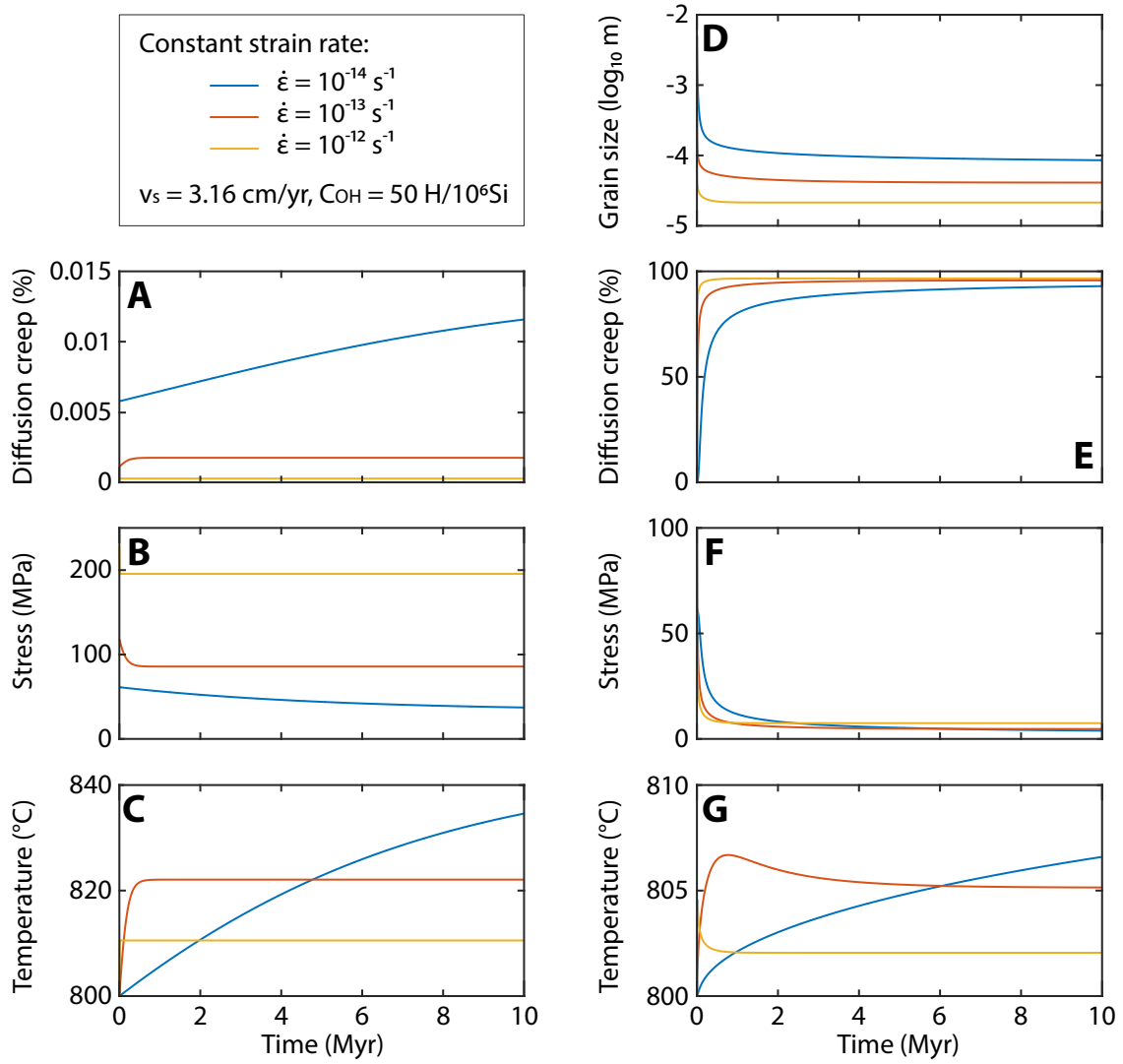

FIGURE 3. Temporal evolution of simulations at constant strain rates at PT conditions of 800°C and 1.65GPa, a shear velocity of 3.16cm/yr and hydrogen concentration of 50H/10^{6}Si. Left column: Constant grain size of 5mm. Right column: Self-consistent grain-size evolution. A, E) Percentage of diffusion creep adding to the total strain rate. B, F) Strain rate. C, G) Temperature. D) Grain size. Colors indicate applied strain rate.

al., 1999) reported significant shear heating along the Ailao Shan–Red River shear zone. There, observed shear heating can be explained by quartz deforming predominantly by grain-size-independent creep, *i.e.* dynamic recrystallization does not necessarily result in mechanical weakening (Stipp *et al.*, 2002a, b). Shear heating in olivine-bearing mantle rocks significant enough for being responsible for the initiation of subduction or continental break up has not been reported yet from natural shear zones.

Limitations of the modelling approach

This study presents a simplified, but physically valid numerical approach coupling composite diffusion-dislocation viscous rheologies with a self-consisting grain-size evolution model with the main goal to demonstrate that grain-size reduction severely affects the ductile strength of olivine-bearing mantle shear zones, leading to a reduction of shear heating in contrast to pure dislocation creep, for example by assuming constant grain sizes. While the effects of grain-size evolution on the thermal and mechanical evolution of a shear zone are evident, the numerical approach does not consider geological conditions or processes such as phase mixing that is followed by increasing strain (Bercovici and Skemer, 2017), chemical reaction (Furusho and Kanagawa, 1999), and melt and/or water infiltration (Kelemen and Dick, 1995). Furthermore, these processes may also play a role in producing or loosing heat. For example, polymineralic systems with phase mixing show hampered grain-growth rates in contrast to mono-mineralic systems without mixing (Bercovici and Ricard, 2012; Herwegh *et al.*, 2011; Linckens *et al.*, 2015;

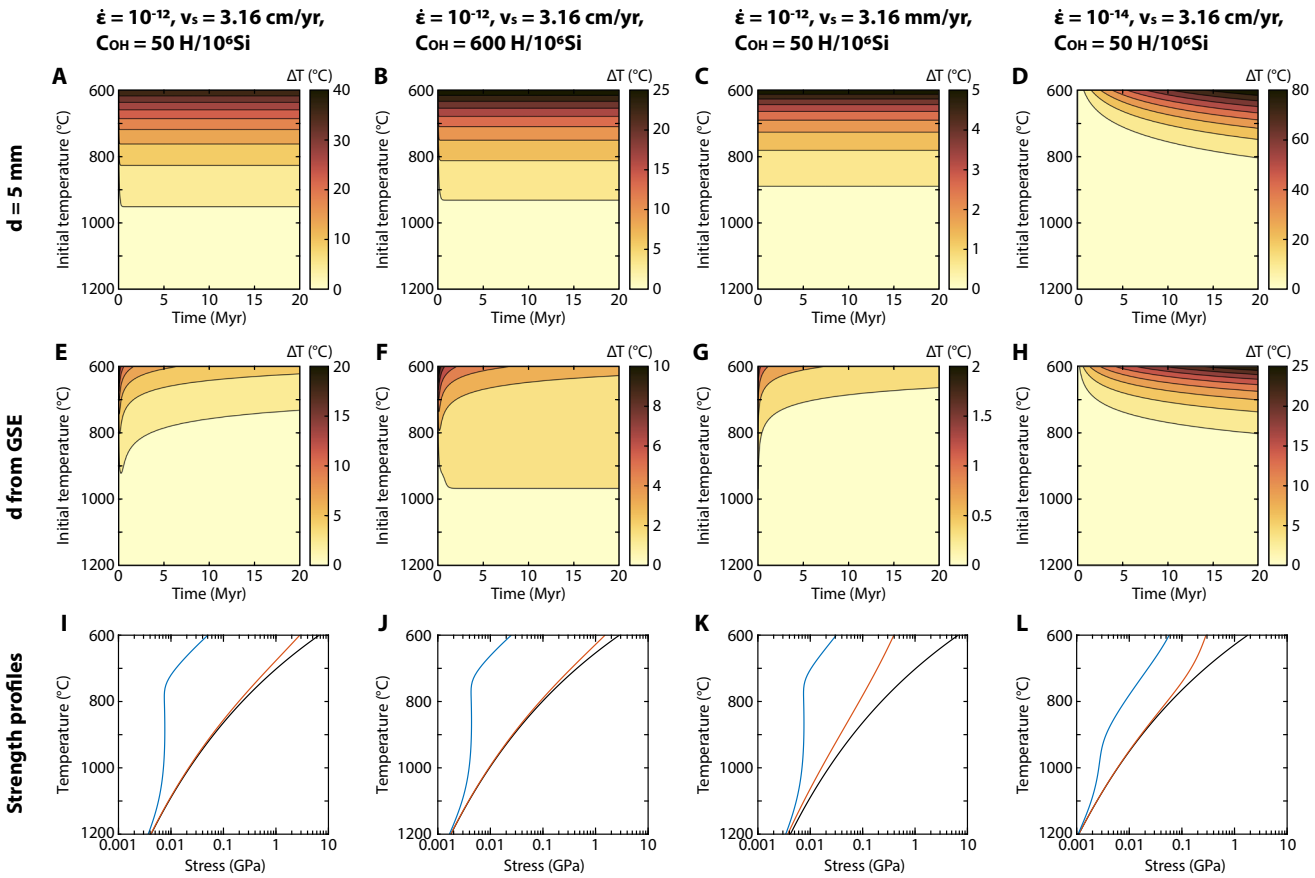

FIGURE 4. A-H) Temporal evolution of the temperature anomaly related to shear heating across mantle-lithospheric PT conditions from 600–1200°C and 1–2.94GPa, respectively. A-D) Constant grain size of 5mm. E-H) Self-consistent grain-size evolution. I-L) Strength profiles at initial conditions (black) and after 2Myr for both constant grain size (red) and grain-size evolution (blue). Applied strain rates, shear velocities and hydrogen concentrations are indicated at the top of each column.

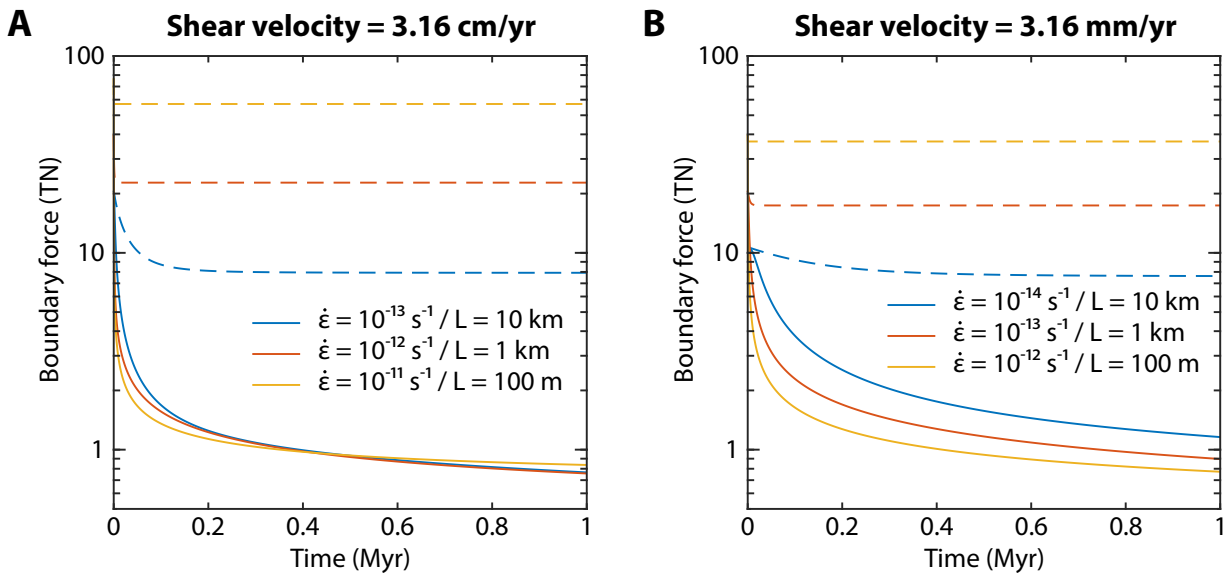

FIGURE 5. Temporal evolution of boundary force for hydrogen concentration of 50H/106Si constrained from strength profiles shown in Figure 4I-L. Dashed lines: Constant grain size of 5mm. Full lines: Self-consistent grain-size evolution model. Colors indicate applied constant strain rates and shear zone width. A) Shear velocity = 3.16cm/yr. B) Shear velocity = 3.16mm/yr.

Linckens *et al.*, 2011). However, the implementation of phase mixing into the equation would result in smaller grain sizes and therefore further diminish the effect of shear heating and therefore not undermining the main argument of this study. In fact, the present work shows that numerical models often exhibiting dislocation creep rheologies for pure olivine generally overestimate shear heating produced along lithospheric shear zones due to the lack of alternative processes of mechanical weakening.

CONCLUSIONS

Many studies interpret shear heating to be an important factor in weakening and localization of deformation in the mantle lithosphere. The presented simulations demonstrate that grain-size reduction is not only a much more efficient weakening process, but it also undermines shear heating due to drastically reduced stresses and hence dissipated mechanical energy along shear zones. Simulations at constant stress reach a steady state, when shear-heating production matches heat loss by diffusion, giving insights into preferred shear zone width and viscosity depending on shear velocity and stress. Simulations at constant strain rate allow constructing strength profiles and calculate acting boundary forces. In contrast to shear heating, a self-consistent grain-size evolution allows for fast (<500kyr) lithospheric weakening that allows sustaining active plate tectonics with strong plates and weak boundaries.

ACKNOWLEDGMENTS

The author thanks the anonymous reviewers for their constructive comments. This work was supported by the projects RYC2021-031331-I, CNS2023-145755, PID2022-139422NB-I00 and CEX2024-001494-S, funded by MICIU/AEI/10.13039/501100011033, FEDER and European Union NextGenerationEU/PRTR.

REFERENCES

Alevizos, S., Poulet, T., Veveakis, E., 2014. Thermo-poro-mechanics of chemically active creeping faults. 1: Theory and steady state considerations. Journal of Geophysical Research-Solid Earth, 119(6), 4558-4582.

Austin, N., Evans, B., 2007. Paleowattmeters: A scaling relation for dynamically recrystallized grain size. Geology, 35(4), 343-346.

Austin, N., Evans, B., 2009. The kinetics of microstructural evolution during deformation of calcite. Journal of Geophysical Research-Solid Earth, 114, .

Behn, M.D., Hirth, G., Elsenbeck, J.R., 2009. Implications of grain size evolution on the seismic structure of the oceanic upper mantle. Earth and Planetary Science Letters, 282(1-4), 178-189.

Bercovici, D., Ricard, Y., 2012. Mechanisms for the generation of plate tectonics by two-phase grain-damage and pinning. Physics of the Earth and Planetary Interiors, 202, 27-55.

Bercovici, D., Skemer, P., 2017. Grain damage, phase mixing and plate-boundary formation. Journal of Geodynamics, 108, 40-55.

Bercovici, D., Ricard, Y., Richards, M., 2000. The relation between mantle dynamics and plate tectonics: A primer. Geophysical Monograph-American Geophysical Union, 121, 5-46.

Bird, P., Liu, Z., Rucker, W.K., 2008. Stresses that drive the plates from below: Definitions, computational path, model optimization, and error analysis. Journal of Geophysical Research-Solid Earth, 113(B11). DOI: Artn B11406 10.1029/2007jb005460

Braun, J., Chery, J., Poliakov, A., Mainprice, D., Vauchez, A., Tommasi, A., Daignieres, M., 1999. A simple parameterization of strain localization in the ductile regime due to grain size reduction: A case study for olivine. Journal of Geophysical Research-Solid Earth, 104(B11), 25167-25181. DOI: 10.1029/1999jb900214

Brun, J.P., Cobbold, P.R., 1980. Strain Heating and Thermal Softening in Continental Shear Zones - a Review. Journal of Structural Geology, 2(1-2), 149-158.

Burg, J.P., Gerya, T.V., 2005. The role of viscous heating in Barrovian metamorphism of collisional orogens: thermomechanical models and application to the Lepontine Dome in the Central Alps. Journal of Metamorphic Geology, 23(2), 75-95. DOI: 10.1111/j.1525-1314.2005.00563.x

Camacho, A., McDougall, I., Armstrong, R., Braun, J., 2001. Evidence for shear heating, Musgrave Block, central Australia. Journal of Structural Geology, 23(6-7), 1007-1013.

Ceccato, A., Menegon, L., Pennacchioni, G., Morales, L.F.G., 2018. Myrmekite and strain weakening in granitoid mylonites. Solid Earth, 9(6), 1399-1419.

Clauser, C., Huenges, E., 1995. Thermal conductivity of rocks and minerals.

Dannberg, J., Eilon, Z., Faul, U., Gassmoller, R., Moulik, P., Myhill, R., 2017. The importance of grain size to mantle dynamics and seismological observations. Geochemistry Geophysics Geosystems, 18(8), 3034-3061.

De Bresser, J.H.P., Ter Heege, J.H., Spiers, C.J., 2001. Grain size reduction by dynamic recrystallization: can it result in major theological weakening? International Journal of Earth Sciences, 90(1), 28-45.

Duretz, T., Schmalholz, S.M., Podladchikov, Y.Y., 2015. Shear heating-induced strain localization across the scales. Philosophical Magazine, 95(28-30), 3192-3207.

Duyster, J., Stöckhert, B., 2001. Grain boundary energies in olivine derived from natural microstructures. Contributions to Mineralogy and Petrology, 140(5), 567-576. DOI: 10.1007/s004100000200

Dygert, N., Bernard, R.E., Behr, W.M., 2019. Great Basin Mantle Xenoliths Record Active Lithospheric Downwelling Beneath

Central Nevada. Geochemistry Geophysics Geosystems, 20(2), 751-772.

Frederiksen, S., Braun, J., 2001. Numerical modelling of strain localisation during extension of the continental lithosphere. Earth and Planetary Science Letters, 188(1-2), 241-251.

Fuchs, L., Becker, T.W., 2021. Deformation Memory in the Lithosphere: A Comparison of Damage-dependent Weakening and Grain-Size Sensitive Rheologies. Journal of Geophysical Research-Solid Earth, 126(1).

Furusho, M., Kanagawa, K., 1999. Transformation-induced strain localization in a Iherzolite mylonite from the Hidaka metamorphic belt of central Hokkaido, Japan. Tectonophysics, 313(4), 411-432.

Gurnis, M., Zhong, S., Toth, J., 2000. On the competing roles of fault reactivation and brittle failure in generating plate tectonics from mantle convection. In: The History and Dynamics of Global Plate Motions. Washington D.C., American Geophysical Union, Geophysical Monograph, 121, 73-94.

Gurnis, M., Hall, C., Lavier, L., 2004. Evolving force balance during incipient subduction. Geochemistry Geophysics Geosystems, 5. DOI: Artn Q07001 10.1029/2003gc000681

Hartz, E.H., Podladchikov, Y.Y., 2008. Toasting the jelly sandwich: The effect of shear heating on lithospheric geotherms and strength. Geology, 36(4), 331-334. DOI: 10.1130/G24424a.1

Herwegh, M., Linckens, J., Ebert, A., Berger, A., Brodhag, S.H., 2011. The role of second phases for controlling microstructural evolution in polymineralic rocks: A review. Journal of Structural Geology, 33(12), 1728-1750.

Hirth, G., Kohlstedt, D., 2003. Rheology of the upper mantle and the mantle wedge: A view from the experimentalists. Geophysical Monograph-American Geophysical Union, 138, 83-106.

Hodowany, J., Ravichandran, G., Rosakis, A.J., Rosakis, P., 2000. Partition of plastic work into heat and stored energy in metals. Experimental Mechanics, 40(2), 113-123.

Holtzman, B.K., Chrysochoos, A., Daridon, L., 2018. A Thermomechanical Framework for Analysis of Microstructural Evolution: Application to Olivine Rocks at High Temperature. Journal of Geophysical Research-Solid Earth, 123(10), 8474-8507.

Holyoke, C.W., Tullis, J., 2006. Formation and maintenance of shear zones. Geology, 34(2), 105-108.

Jain, C., Korenaga, J., Karato, S.I., 2018. On the Grain Size Sensitivity of Olivine Rheology. Journal of Geophysical Research-Solid Earth, 123(1), 674-688.

Jin, Z.M., Zhang, J., Green, H.W., Jin, S., 2001. Eclogite rheology: Implications for subducted lithosphere. Geology, 29(8), 667-670.

Karato, S., 1989. Grain-Growth Kinetics in Olivine Aggregates. Tectonophysics, 168(4), 255-273.

Kaus, B.J.P., Podladchikov, Y.Y., 2006. Initiation of localized shear zones in viscoelastoplastic rocks. Journal of Geophysical Research-Solid Earth, 111(B4). DOI: Artn B04412 10.1029/2005jb003652

Kelemen, P.B., Dick, H.J.B., 1995. Focused Melt Flow and Localized Deformation in the Upper-Mantle - Juxtaposition of Replacive Dunite and Ductile Shear Zones in the Josephine Peridotite, Sw Oregon. Journal of Geophysical Research-Solid Earth, 100(B1), 423-438.

Kiss, D., Candioti, L.G., Duretz, T., Schmalholz, S.M., 2020. Thermal softening induced subduction initiation at a passive margin. Geophysical Journal International, 220(3), 2068-2073.

Leloup, P.H., Kienast, J.R., 1993. High-Temperature Metamorphism in a Major Strike-Slip Shear Zone - the Ailao-Shan-Red River, Peoples-Republic-of-China. Earth and Planetary Science Letters, 118(1-4), 213-234.

Leloup, P.H., Ricard, Y., Battaglia, J., Lacassin, R., 1999. Shear heating in continental strike-slip shear zones: model and field examples. Geophysical Journal International, 136(1), 19-40.

Linckens, J., Herwegh, M., Muntener, O., Mercolli, I., 2011. Evolution of a polymineralic mantle shear zone and the role of second phases in the localization of deformation. Journal of Geophysical Research-Solid Earth, 116.

Linckens, J., Herwegh, M., Muntener, O., 2015. Small quantity but large effect - How minor phases control strain localization in upper mantle shear zones. Tectonophysics, 643, 26-43.

Mako, C.A., Caddick, M.J., 2018. Quantifying magnitudes of shear heating in metamorphic systems. Tectonophysics, 744, 499-517.

Montesi, L.G.J., 2013. Fabric development as the key for forming ductile shear zones and enabling plate tectonics. Journal of Structural Geology, 50, 254-266. DOI: 10.1016/j.jsg.2012.12.011

Oliot, E., Goncalves, P., Marquer, D., 2010. Role of plagioclase and reaction softening in a metagranite shear zone at mid-crustal conditions (Gotthard Massif, Swiss Central Alps). Journal of Metamorphic Geology, 28(8), 849-871.

Platt, J.P., 2015. Influence of shear heating on microstructurally defined plate boundary shear zones. Journal of Structural Geology, 79, 80-89.

Platt, J.P., Behr, W.M., 2011. Grainsize evolution in ductile shear zones: Implications for strain localization and the strength of the lithosphere. Journal of Structural Geology, 33(4), 537-550. DOI: 10.1016/j.jsg.2011.01.018

Rast, M., & Ruh, J. B. (2021). Numerical shear experiments of quartz-biotite aggregates: Insights on strain weakening and two-phase flow laws. *Journal of Structural Geology, 149*.

Ruh, J.B., Tokle, L., Behr, W.M., 2022. Grain size evolution controls on lithospheric weakening during continental rifting. Nature Geoscience.

Ruh, J., Behr, W., Tokle, L.J.T., 2024. Effect of Grain-Size and Textural Weakening in Polyphase Crustal and Mantle Lithospheric Shear Zones. 2(1), 91-110.

Schierjott, J.C., Thielmann, M., Rozel, A.B., Golabek, G.J., Gerya, T.V., 2020. Can Grain Size Reduction Initiate Transform Faults?-Insights From a 3-D Numerical Study. Tectonics, 39(10).

Schmalholz, S.M., Duretz, T., 2015. Shear zone and nappe formation by thermal softening, related stress and temperature evolution, and application to the Alps. Journal of Metamorphic Geology, 33(8), 887-908.

Spang, A., Thielmann, M., Kiss, D., 2024. Rapid Ductile Strain Localization Due To Thermal Runaway. Journal of Geophysical Research-Solid Earth, 129(10). DOI: ARTN e2024JB028846 10.1029/2024JB028846

Spang, A., Thielmann, M., de Montserrat, A., Duretz, T., 2025. Transient Propagation of Ductile Ruptures by Thermal Runaway. Journal of Geophysical Research-Solid Earth, 130(6). DOI: ARTN e2025JB031240 10.1029/2025JB031240

Speciale, P.A., Behr, W.M., Hirth, G., Tokle, L., 2020. Rates of Olivine Grain Growth During Dynamic Recrystallization and Postdeformation Annealing. Journal of Geophysical Research-Solid Earth, 125(11).

Stipp, M., Stunitz, H., Heilbronner, R., Schmid, S.M., 2002a. Dynamic recrystallization of quartz: correlation between natural and experimental conditions. London, The Geological Society, 200(1, Special Publications), 171-190.

Stipp, M., Stunitz, H., Heilbronner, R., Schmid, S.M., 2002b. The eastern Tonale fault zone: a 'natural laboratory' for crystal plastic deformation of quartz over a temperature range from 250 to 700 degrees C. Journal of Structural Geology, 24(12), 1861-1884.

Thielmann, M., Kaus, B.J.P., 2012. Shear heating induced lithospheric-scale localization: Does it result in subduction? Earth and Planetary Science Letters, 359, 1-13. DOI: 10.1016/j.epsl.2012.10.002

Thielmann, M., Rozel, A., Kaus, B.J.P., Ricard, Y., 2015. Intermediate-depth earthquake generation and shear zone formation caused by grain size reduction and shear heating. Geology, 43(9), 791-794.

Tokle, L., Hirth, G., 2021. Assessment of Quartz Grain Growth and the Application of the Wattmeter to Predict Quartz Recrystallized Grain Sizes. Journal of Geophysical Research-Solid Earth, 126(7).

Turcotte, D.L., Schubert, G., 2002. Geodynamics: Cambridge university press.

Warren, J.M., Hirth, G., 2006. Grain size sensitive deformation mechanisms in naturally deformed peridotites. Earth and Planetary Science Letters, 248(1-2), 438-450.

Wibberley, C.A.J., Shimamoto, T., 2005. Earthquake slip weakening and asperities explained by thermal pressurization. Nature, 436(7051), 689-692.

Yuen, D.A., Fleitout, L., Schubert, G., Froidevaux, C., 1978. Shear Deformation Zones Along Major Transform Faults and Subducting Slabs. Geophysical Journal of the Royal Astronomical Society, 54(1), 93-119.

Manuscript received May 2025;
revision accepted September 2025;
published Online November 2025.